Nanocrystalline CuOx Thin Films for Electrochemical Water Splitting

Ermeson David Santos Silva *, Fernanda Thamiles de Jesus Serrão, Gustavo Henrique dos Santos Domingos, Thiago Mielle Brito Ferreira Oliveira, Marco Aurélio Liutheviciene Cordeiro

Posted Date: 23 May 2024

doi: 10.20944/preprints202405.1556.v1

Keywords: CuOx; Hydrogen evolution; Oxygen evolution;

 doi:10.20944/preprints202405.1556.v1

Article

Nanocrystalline CuO_x Thin Films for Electrochemical Water Splitting

Ermeson D. S. Silva [1,*], Fernanda T. J. Serrão [1,], Gustavo H. S. Domingos [1,], Thiago M. B. F. Oliveira [3,], Marco A. L. Cordeiro [1,]

[1] Graduate Program in Materials Science and Engineering, Federal University of São Carlos, Rod. Washington Luis, s/n, São Carlos 13565-905, Brazil
[2] Centro de Ciência e Tecnologia, Universidade Federal do Cariri, Av. Tenente Raimundo Rocha, 1639, Cidade Universitária, Juazeiro do Norte 63048-080, CE, Brazil
* Correspondence: ermeson.silva@estudante.ufscar.br

Abstract: New advances in creating effective and affordable copper-based catalysts for water splitting represent a promising strategy for driving sustainable energy technologies. However, materials containing copper are susceptible to corrosion and agglomeration. In this study, we describe a synthesis route to produce olamine-functionalized CuO nanoparticles using the Hot Injection method. Nanoparticles were obtained and subsequently deposited on FTO substrates, undergoing thermal treatment at 500°C and 600°C in atmospheres containing O_2 and N_2, aiming to enhance the adhesion of the active material to the substrate and modify its oxidation state. Microstructural properties were analyzed using XRD, SEM, and TEM, while electrochemical properties were studied using CV, LSV, and EIS. Electrodes treated thermally in an N_2 atmosphere at 600°C exhibited higher ESCA, indicating a greater area of active sites exposed to surface reactions and, therefore, superior catalytic activity in Hydrogen Evolution Reaction (HER). These findings show an interesting strategy for avoiding rapid electron-hole recombination and, consequently, CuO corrosion. For Oxygen Evolution Reaction (OER), samples treated thermally in O_2 atmosphere at 500°C and 600°C appear to be more effective.

Keywords: CuO_x; Hydrogen evolution; Oxygen evolution;

1. Introduction

According to recent projections, the global population is expected to reach approximately 10.4 billion by 2080, exacerbating social, health, and environmental issues [**?**], coupled with growing pressures on industrial production, livestock farming, urban mobility and energy demand, which are increasing by the production of greenhouse gases [**?**]. As fossil fuels continue to diminish, their ecological impact and the increasing energy needs are driving a projected transition to alternative energy sources [**? ?**].

In this context, hydrogen (H_2) holds significant potential due to its high energy content. Among the methods for hydrogen production, water electrolysis into hydrogen and oxygen, driven by luminous energy (i.e., photo-promoted) allies with electrical energy (i.e., electro-promoted), transforms water into an inexhaustible and environmentally friendly fuel source [**? ? ?**]. This strategy is one of the easiest way to implement in industries [**? ?**].

Copper oxide (CuO_x) stands out as a p-type semiconductor with band-gap energies favorable to the use of visible light, low cost, abundance on Earth's crust, non-toxicity, and relatively high charge carrier mobility among similar oxides, making it advantageous for its use in the conversion of solar energy into hydrogen [**? ?**]. However, several challenges still need to be overcome for the use of copper oxides as photocathodes in H_2 production through water splitting, notably concerning structural stabilization (susceptibility to corrosion), and high electron-hole recombination (leading to a shorter mean free path in charge carrier diffusion) and agglomeration [**?**]. An effective strategy to ensure the electrochemical stability of working electrodes and reduce agglomeration is to employ organic layers containing oleate groups.

 doi:10.20944/preprints202405.1556.v1

In this scenario, CuO_x nanoparticles were obtained via Hot Injection Method and subsequently deposited on an FTO substrate, followed by a thermal treatment to enhance adhesion between the substrate and the material. The performance of this material was then evaluated with the aim of its application as electrocatalysts in HER and OER processes.

2. Materials and Methods

2.1. Reagents and Materials

Copper acetate [$Cu(CO_2CH_3)_2$] (Êxodo Científica, 97% purity), oleylamine [$C_{18}H_{35}NH_2$] (Sigma-Aldrich, 97% purity), isopropyl alcohol [C_3H_8O] (Synth, 100% purity), chloroform [$CHCl_3$] (Honeywell, 99% purity), ethyl alcohol [CH_3CH_2OH] (Synth, 95% purity), and toluene $C_6H_5CH_3$] (Honeywell, 99% purity) were used.

2.2. Copper Nanoparticles (NPs) Synthesis

First, 0.5g of copper (II) acetate ([$Cu(CO_2CH_3)_2$]) was dissolved in 10ml of oleylamine [$C_{18}H_{35}NH_2$] (OAm) through constant stirring at 40°C for 30 minutes. The resulting solution was then transferred to a glass syringe. In parallel, 15ml of oleylamine were added to a three-necked flask equipped with magnetic stirring and heated until it reached 310°C. When the desired temperature was reached, the syringe containing the prepared solution was introduced into the flask, resulting in a decrease in the system temperature. After waiting for the temperature to return to 310°C, the synthesis process was continued and maintained for 40 minutes, thus concluding the synthesis stage. At the end of the reaction time, functionalized CuO nanoparticles were obtained and dispersed in oleylamine. To separate the hybrid structures, the nanoparticles were subjected to four washes using a solvent mixture composed of toluene and ethanol in a 1:1 ratio. After each wash, the material was centrifuged at 3800 rpm for 10 minutes. After the washing process and obtaining the precipitate, the nanoparticle suspension was redispersed in toluene.

2.3. Development of Electrocatalysts

A fluorine-doped tin oxide (FTO;7 Ω/sq) electrode was used as support, after cleaning in isopropyl alcohol, followed by an ultrasonic bath for 5 minutes and washed again with isopropyl alcohol. The modifier was produced from a colloidal suspension of CuO nanoparticles in toluene, deposited using the dip-coating technique in an area of 1.0 cm^2. For each deposition, the substrate was introduced into the colloid at a speed of 5 mm/s, remained immersed for 10s and finally removed at a speed of 5 mm/s. After removing the previous layer with chloroform, the solvent was evaporated leaving the substrate under a thermal blanket at 140°C for 1 min. The deposition scheme is illustrated in Figure **??** and was repeated 15 times. Therefore, the deposited films were heat treated at 500°C or 600°C for 1.5 h, both in air and in a nitrogen atmosphere. The samples were described as follows: "C" for the deposited copper, followed by the temperature (500°C or 600°C), and "A" if the heat treatment occurred in an oxidizing atmosphere, and "N" if it occurred in a nitrogen atmosphere.

 doi:10.20944/preprints202405.1556.v1

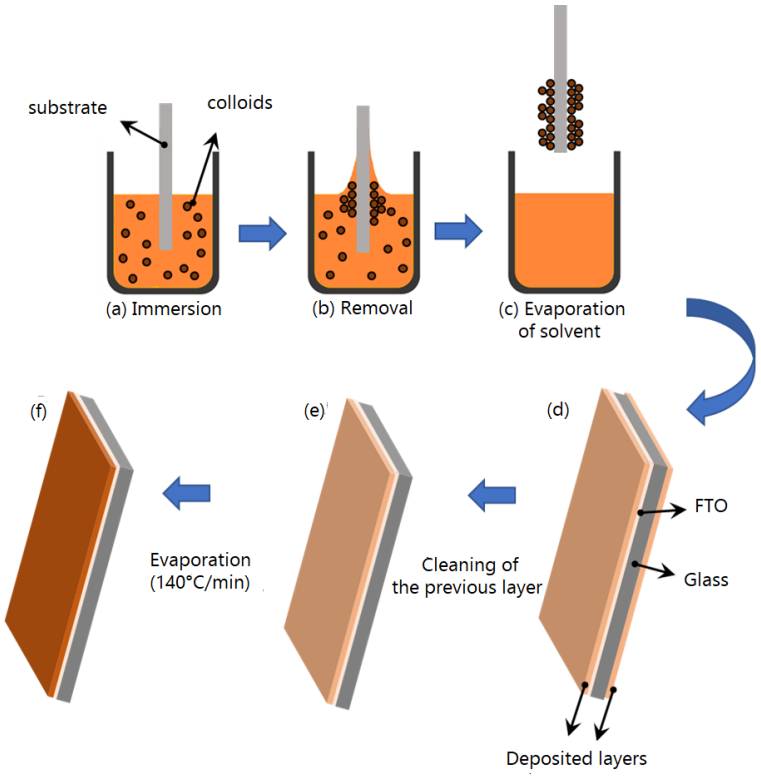

Figure 1. (a)-(b) Scheme of deposition of CuO particles on the substrate by dip-coating; (d)-(e) substrate treatment sequence after deposition.

2.4. Characterization

Voltammetric and impedimetric data were obtained by a modular potentiostat/galvanostat (PGSTAT 128 N/FRA32, Metrohm-Autolab, The Netherlands). Morphological aspects of the materials were evaluated with a scanning electron microscope (SEM; FEI Magellan 400L, Japão) and transmission electron microscopy (TEM, FEI TECNAI G2 S-TWIN) The crystallinity and purity of the materials were verified by X-ray diffraction (XRD; Bruker D8 Advance XRD diffractometer, Germany), using CuKα radiation (λ = 1.5418 Å) in the 2θ range from 10° to 90°.

3. Results and Discussion

3.1. General Features of the Electrodic Materials

The diffractogram of the synthesized nanoparticles (Figure **??**) demonstrated the monoclinic crystalline phase of CuO, with characteristic peaks of this structure at 35.5º, 37.8º, 49º, 54º, 61.8º, and 66.6º (PDF 041-0254) correspond to (111), (111), (202), (202), (113), (310) crystal planes of CuO, respectively, indicating the presence of this crystalline phase with the metallic cation in a higher oxidation state due to the presence of oxygen in the reaction medium. Additionally, a lower peak resolution and signal-to-noise ratio are observed, suggesting the presence of an amorphous component in the material resulting from oleate groups on the particle surfaces. The average crystallite size was calculated from the diffractogram analysis using the Scherrer equation, demonstrating that the average crystallite size was 6.9 nm.

 doi:10.20944/preprints202405.1556.v1

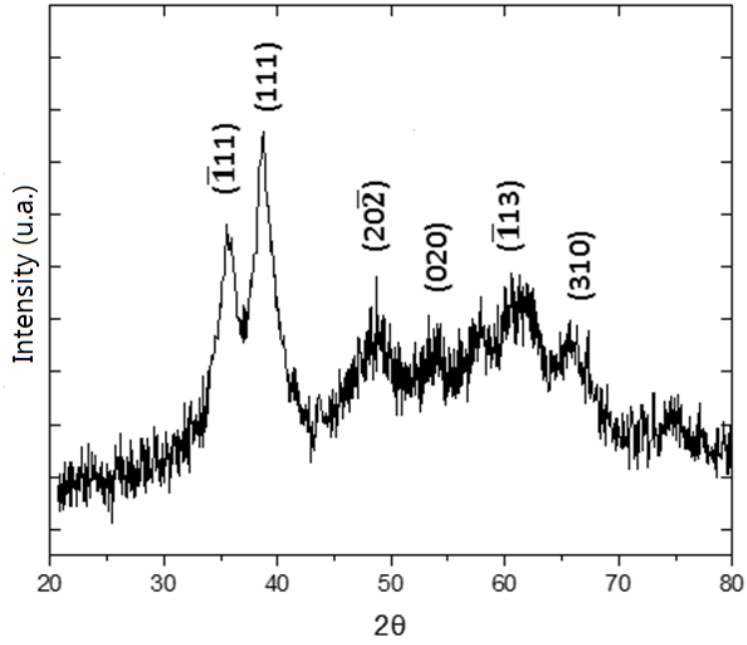

Figure 2. X-ray diffractogram of synthesized CuO nanoparticles.

The XRD patterns of the thin films prepared under air and nitroges atmospheres (Figure **??**), shows characteristic peaks are observed at approximately 26.5°, 33.7°, 37.7°, 51.7°, 61.7°, and 65.70° 2θ angles. These peaks are attributed to the presence of $SnO_2 : F(FTO)$, acting as the substrate (PDF – 46-1088). Additionally, characteristic peaks are identified at approximately 35.6° (111), 38.7° (002), 48.7° (020), 61.5° (202), and 66.2° (113), indicative of the presence of CuO in the films (PDF – 40-1132). Furthermore, some characteristic peaks are also observed at 2θ angles around 36.4° (110), 42.4° (111), 61.3° (220), and 73.8° (311), attributed to the presence of Cu_2O, which are more pronounced in samples subjected to thermal treatment under a nitrogen atmosphere (JCPDS 04-007-9767).

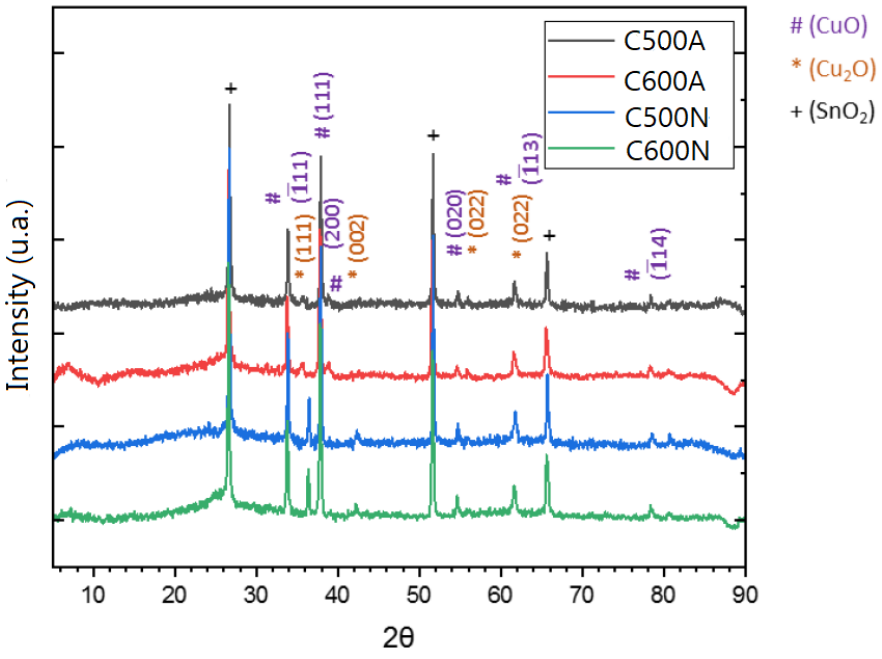

Figure 3. X-ray diffractogram for the systems heat-treated at 500°C and 600°C in air and nitrogen atmosphere.

 doi:10.20944/preprints202405.1556.v1

Sample morphologies were determined by TEM. Figure **??**a depicts the formation of dispersed nanoparticles, with an average size of 7 nm, in accordance with that determined by the Scherrer equation. Additionally, Fig **??**b shows an image of an isolated nanoparticle at higher magnification, revealing interplanar spacings of 0.23 nm, corresponding to the 111 family of crystal planes. Overall, the studies presented in the literature indicate CuO particle sizes larger than those found in this study [**?**].

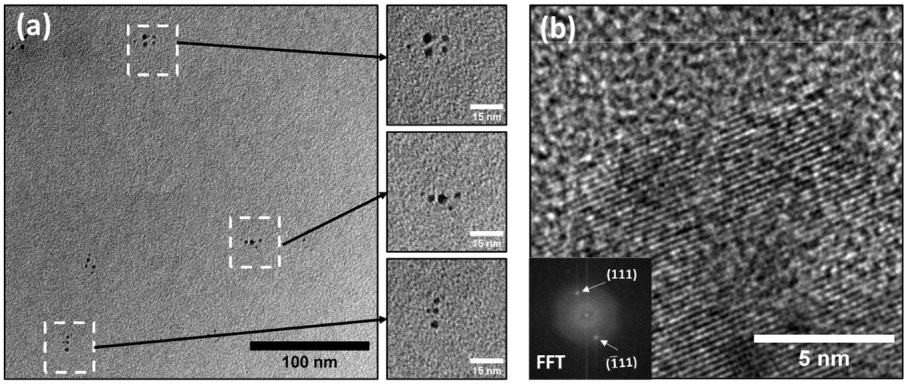

Figure 4. Transmission electron microscopy images of the synthesized CuO nanoparticles, highlighting some groups of structures. (a) Image at lower magnification; (b) Image at higher magnification showing the crystalline planes (111), as indicated by the FFT (inserted in the image).

The sample morphologies were analyzed using SEM. Figure **??** displays FTO with a notably textured surface, composed of clearly defined crystalline grains. This unique morphological structure suggests optimized crystalline orientation, promoting both electrical conduction and light transmission, thus supporting the material's excellence.

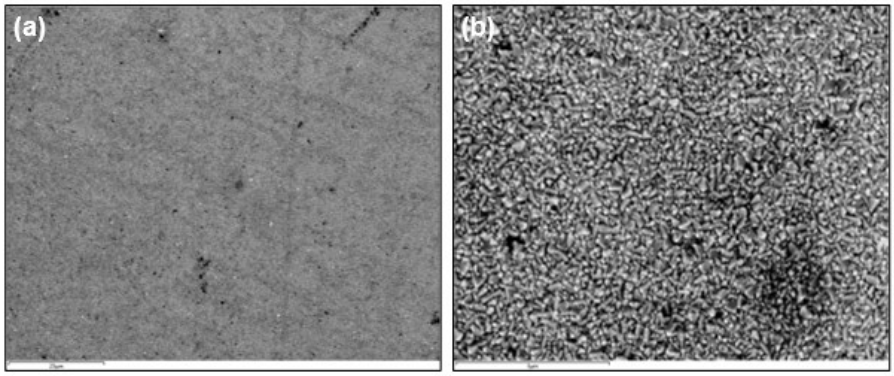

Figure 5. SEM images of the morphology of FTO.

Figure **??**a shows that the surface of the FTO is completely coated with CuO, and Figure **??**b illustrates that the deposited material exhibits agglomerated spheres, although not perfectly defined, positioned close to each other. Remarkably, in Figure **??** (c-d), the same characteristics observed in Figure **??** (a-b) are presented. However, upon magnifying the image, it is noted that the change from an oxygen atmosphere to nitrogen during the thermal treatment resulted in slightly denser particles compared to those observed under an oxygen atmosphere. In Figure **??** (e-f), where the material underwent a thermal treatment at 600°C, there is a noticeable aggregation of particles. This feature indicates a decrease in the individual morphological distinction of the particles, favoring, in turn, greater cohesion among them. This phenomenon suggests that the increase in thermal treatment temperature directly influences the material's cohesion, resulting in a more compact and potentially

 doi:10.20944/preprints202405.1556.v1

more robust structure. Figure **??** (g-h) demonstrates that the change from an oxygen atmosphere to nitrogen during the thermal treatment also resulted in slightly denser particles compared to those observed under an oxygen atmosphere at a temperature of 500°C.

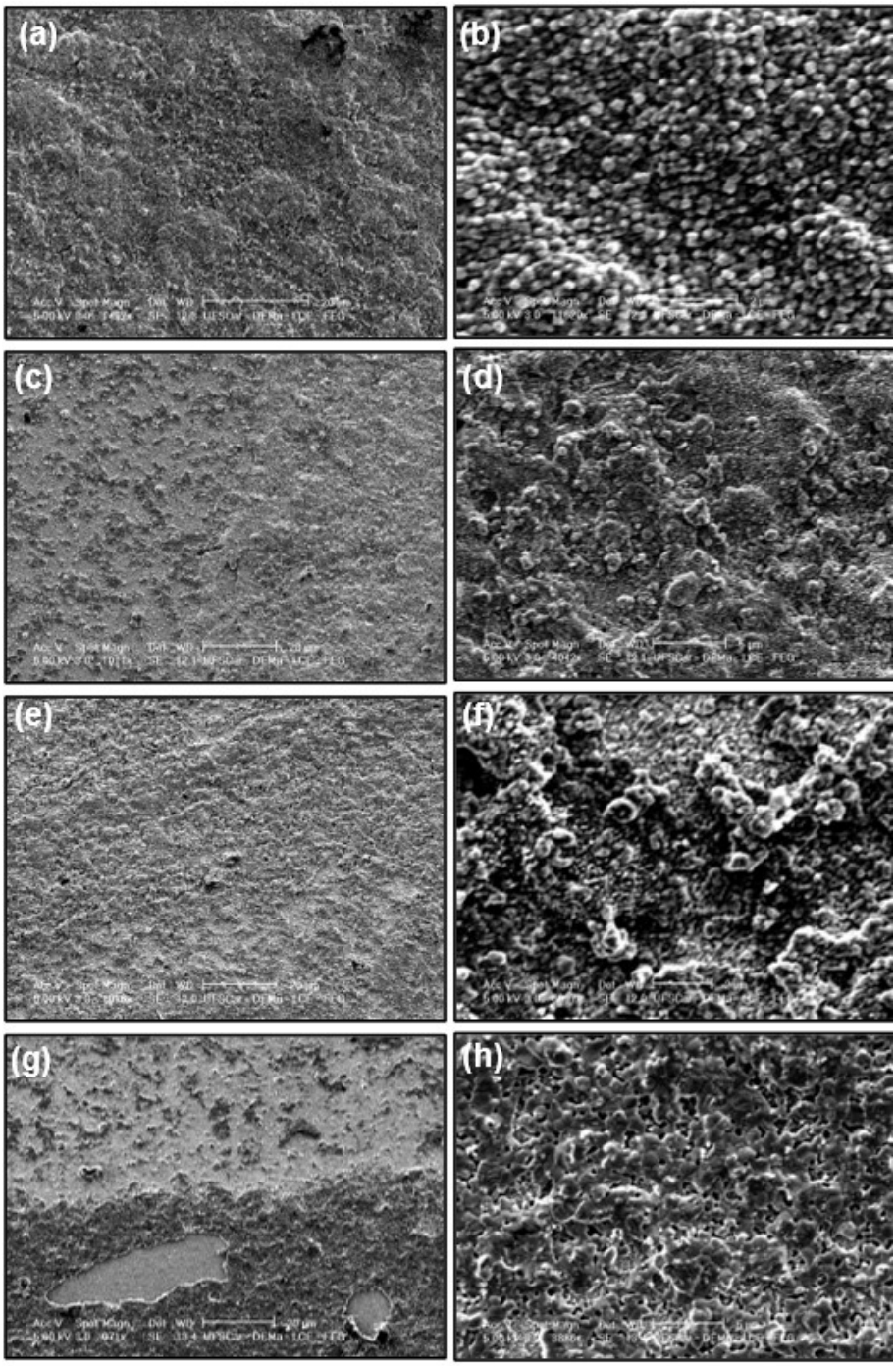

Figure 6. SEM images of the morphology and details of the materials obtained (a-b) C500A, (c-d) C500N, (e-f) C600A, (g-h) C600N.

The electrocatalytic performances of the electrodes were evaluated by measuring the linear sweep voltammetry (LSV) in a 1M KOH alkaline electrolyte. As shown in Figure **??** (left), all samples exhibited superior catalytic activity for HER compared to pure FTO. Notably, the C600N sample stood out by presenting even more enhanced catalytic activity for HER compared to the other samples. This is attributed to the observation that the material on the electrode displayed a red color, potentially

 doi:10.20944/preprints202405.1556.v1

suggesting the formation of Cu_2O instead of CuO, which is typically associated with a black color. This result supports the literature that considers Cu_2O as a promising material for water electrolysis (both through computational simulations and catalytic testing) and is even more effective under certain pH conditions and specific electrical potentials. As evidenced in Figure **??** (right), all samples demonstrated superior catalytic activity for OER compared to pure FTO. Notably, the C600A and C500A samples excelled, displaying even more enhanced catalytic activity for OER compared to the other samples. It is observed that changing the atmosphere to nitrogen apparently improves hydrogen production, unlike the effect on oxygen production. In the case of oxygen production, samples thermally treated in oxygen show a higher capacity.

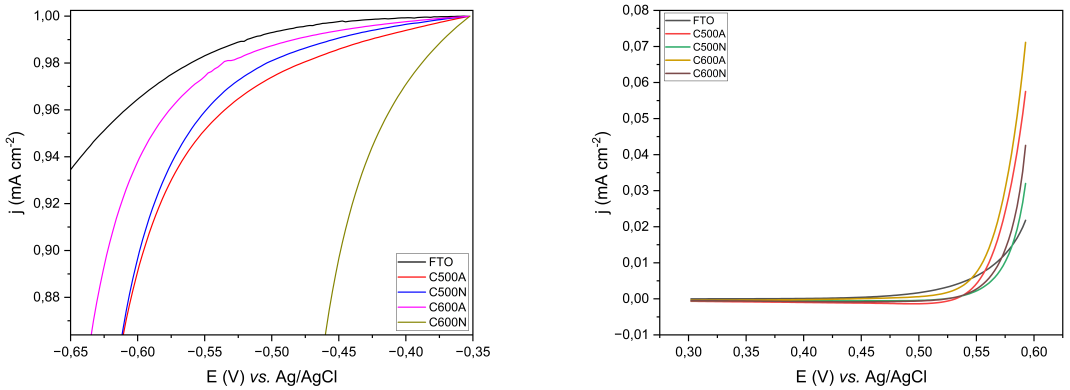

Figure 7. LSV curve in 0.1 M KOH for the working electrodes in relation to hydrogen evolution (left) and oxygen evolution (right).

These results are supported by the electrochemical active surface area (ECSA) values (Figure **??**), where the highest was 2.0E-05 for C500N, followed by 1.9E-05 for both C600N and C600A, and 1.8E-05 for C500A. Higher ECSA values indicate excellent performance; these results highlight the diversity in characteristics and performance among the samples studied. Notably, the C500N sample, having the highest number of exposed active sites for surface reactions, likely contributes to its enhanced performance in hydrogen and oxygen evolution reactions (HER and OER).

 doi:10.20944/preprints202405.1556.v1

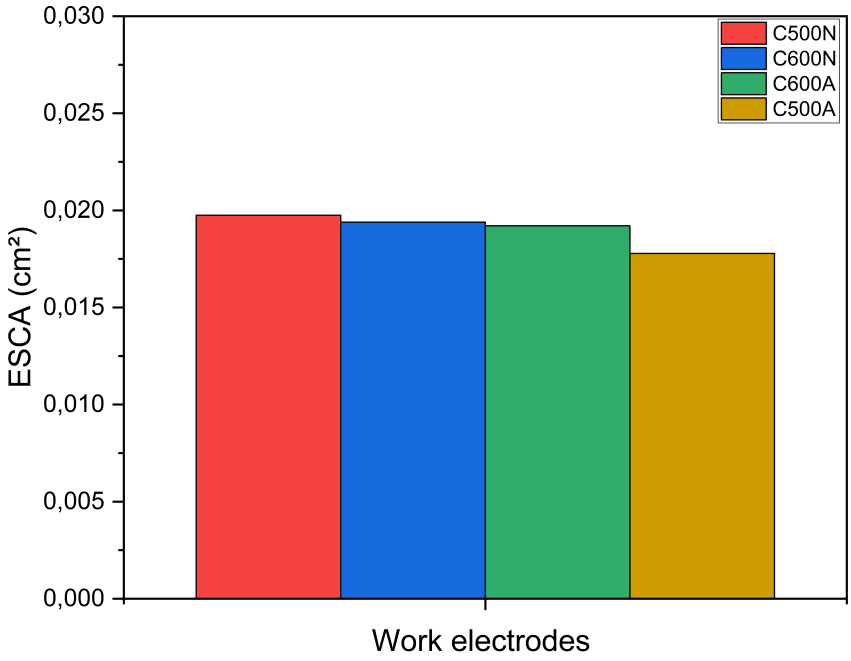

Figure 8. ECSA values for the working electrodes.

Impedance spectra of both electrodes were evaluated by applying a potential of 0.23V in an electrolyte containing $K_4[Fe(CN)_6]$ dissolved in 0.2 M KCl. Subsequently, a simplified model was used to describe the impedance of all electrodes based on an equivalent circuit model in the standard configuration [R([RW]Q)] (attached to the image). It can be observed in Figure **??** that the electrodes display a single semicircle, reflecting the impedance of the system. Following this stage, a resumption of the arc is noted, indicating the onset of diffusional processes. The modification of CuO films under an oxygen atmosphere was crucial in reducing the total charge transfer resistance and increasing the capacitance of the surface states compared to FTO. This was because oxygen may have created pores in the films, thereby increasing the material's surface area. However, the C500N sample (treated thermally in a nitrogen atmosphere) exhibited behavior similar to FTO. Furthermore, an increase was observed in both the total charge transfer resistance and the capacitance of the surface states of the film annealed at 600°C in a nitrogen atmosphere.

 doi:10.20944/preprints202405.1556.v1

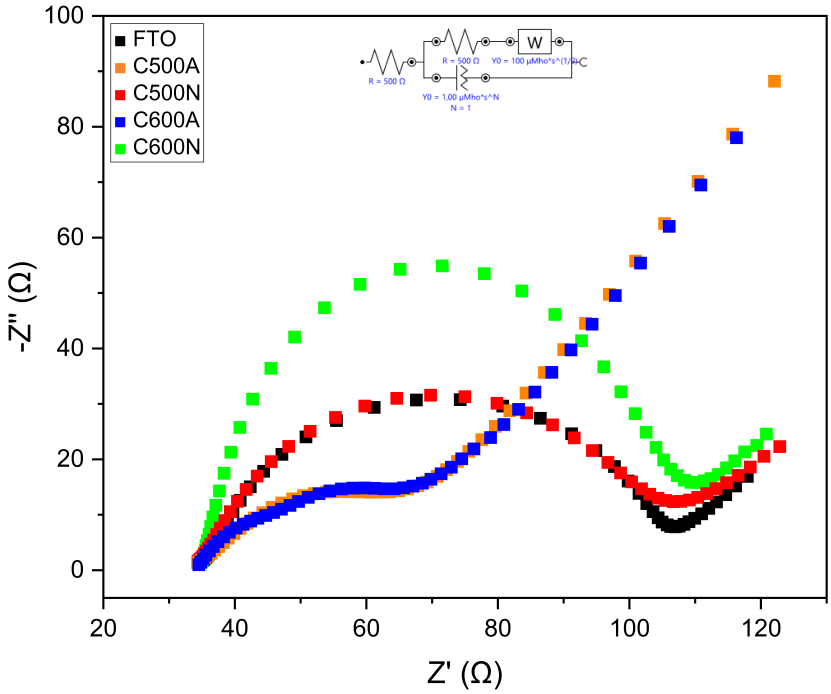

Figure 9. Nyquist plots for the working electrodes.

4. Conclusions

Nanoparticles of CuO functionalized with oleylamine were obtained in a single step through the thermolysis of organometallic precursors. After deposition and thermal treatment at 600°C, both in oxygen and nitrogen atmospheres, the material exhibited densification and agglomeration. Although XRD revealed characteristic peaks associated with the FTO substrate, some samples showed distinctive peaks of CuO and Cu_2O, indicating material deposition on the FTO. Samples thermally treated at 600°C in nitrogen atmosphere, showed great potential for hydrogen and samples thermally treated in air atmosphere, showed great potential for and oxygen evolution reactions, demonstrating versatility. ESCA studies identified that the sample thermally treated at 500°C in a nitrogen atmosphere, exhibited a larger electrochemically active area, suggesting a greater number of active sites exposed to surface reactions, which may contribute to enhancing the performance of hydrogen and oxygen evolution reactions.

Data Availability Statement: The authors declare that they have no known competing financial interests or personal relationships that could have appeared to influence the work reported in this paper.

Acknowledgments: The authors thanks the following Brazilian research financing institution for financial support: The National Council for Scientific and Technological Development – (CNPq) - Finance code (131331/2021-3).

References

. Greguš, J. Sustainability, Population and Reproductive Ethics. *Česká gynekologie* **2023**, *88*, 190–199. doi:10.48095/cccg2023190.
. IEA, P. World Energy Outlook 2021. *https://www.iea.org/reports/world-energy-outlook-2021* **2021**.
. Detz, R.J.; Reek, J.N.H.; van der Zwaan, B.C.C. The future of solar fuels: when could they become competitive? *Energy Environ. Sci.* **2018**, *11*, 1653–1669. doi:10.1039/C8EE00111A.

. Poizot, P.; Dolhem, F. Clean energy new deal for a sustainable world: from non-CO2 generating energy sources to greener electrochemical storage devices. *Energy Environ. Sci.* **2011**, *4*, 2003–2019. doi:10.1039/C0EE00731E.

. Kudo, A.; Miseki, Y. Heterogeneous photocatalyst materials for water splitting. *Chem. Soc. Rev.* **2009**, *38*, 253–278. doi:10.1039/B800489G.

. Kanan, M.W.; Surendranath, Y.; Nocera, D.G. Cobalt–phosphate oxygen-evolving compound. *Chem. Soc. Rev.* **2009**, *38*, 109–114. doi:10.1039/B802885K.

. Luo, S.P.; Mejía, E.; Friedrich, A.; Pazidis, A.; Junge, H.; Surkus, A.E.; Jackstell, R.; Denurra, S.; Gladiali, S.; Lochbrunner, S.; Beller, M. Photocatalytic water reduction with copper-based photosensitizers: a noble-metal-free system. *Angewandte Chemie (International ed. in English)* **2013**, *52*, 419—423. doi:10.1002/anie.201205915.

. Buttler, A.; Spliethoff, H. Current status of water electrolysis for energy storage, grid balancing and sector coupling via power-to-gas and power-to-liquids: A review. *Renewable and Sustainable Energy Reviews* **2018**, *82*, 2440–2454. doi:10.1016/j.rser.2017.09.00.

. Nandy, S.; Banerjee, A.; Fortunato, E.; Martins, R. A Review on Cu2O and CuI-Based p-Type Semiconducting Transparent Oxide Materials: Promising Candidates for New Generation Oxide Based Electronics. *Reviews in Advanced Sciences and Engineering (ISSN: 2157-9121)* **2013**, *2*, 273–304. doi:10.1166/rase.2013.1045.

. Bi, X.; Wang, H.; Yang, Z.; Zhao, Y.; Ma, Z.; Liu, T.; Wu, M. Localized Surface Plasmon Resonance Enhanced Continuous Flow Photoelectrocatalytic CO 2 Conversion to CO. *Energy & Fuels* **2022**, *36*. doi:10.1021/acs.energyfuels.2c01520.

. Kunturu, P.P.; Huskens, J. Efficient Solar Water Splitting Photocathodes Comprising a Copper Oxide Heterostructure Protected by a Thin Carbon Layer. *ACS Applied Energy Materials* **2019**, *2*, 7850–7860, [https://doi.org/10.1021/acsaem.9b01290]. doi:10.1021/acsaem.9b01290.

. Effenberger, F.; Sulca, M.; Machini, M.T.; Couto, R.; Kiyohara, P.; Machado, G.; Rossi, L. Copper nanoparticles synthesized by thermal decomposition in liquid phase: the influence of capping ligands on the synthesis and bactericidal activity. *Journal of Nanoparticle Research* **2014**, *16*, 2588. doi:10.1007/s11051-014-2588-7.